Suspension of active rod-like particles in complex flows

Hamza Issa, Giovanniantonio Natale, Gilles Ausias, Julien Férec

Suspension of active rod-like particles in complex flows

Hamza Issa
Univ. Bretagne Sud, UMR CNRS 6027, IRDL, F-56100 Lorient, France
Department of Chemical and Petroleum Engineering, Schulich School of Engineering, University of Calgary, 2500 University Drive NW, T2N 1N4, Canada

Giovanniantonio Natale
Department of Chemical and Petroleum Engineering, Schulich School of Engineering, University of Calgary, 2500 University Dr. NW, T2N 1N4, Canada

Gilles Ausias
Univ. Bretagne Sud, UMR CNRS 6027, IRDL, F-56100 Lorient, France

Julien Férec
Univ. Bretagne Sud, UMR CNRS 6027, IRDL, F-56100 Lorient, France
(Dated: November 26, 2024)

This study explores the dynamics of active rodlike particles in flow systems, focusing on the active particles-fluid interactions and particles accumulation induced by anisotropic translational diffusion. Numerical simulations based on the work of Mezi et al. [1] are used to analyse the results. In Poiseuille flow, active rods are accumulated at the walls with high alignment in the flow direction and nematic order in the wall directions. A circular obstacle is introduced in the Poiseuille flow which develops non-homogeneous flow. The results of this study offer important new understandings into the intricate behavior of suspended active rods under various flow conditions.

I. INTRODUCTION

The movement of active particles within confined spaces and their interaction with solid boundaries are crucial in various biological processes. Spermatozoa accumulate at surfaces [2], which is important for sperm behavior and interactions during fertilization. Bacterias tend to gather and interact with external flows near surfaces, significantly impacting their adhesion and biofilm formation capabilities. Lecuyer et al. [3] found that Pseudomonas aeruginosa PA14 bacteria stick to surfaces for longer time with increasing shear stress. Additionally, the concentration of bacteria near surfaces affects how they interact with the gastrointestinal wall during digestion, which has implications for a number of pathologies [4, 5]. The tendency of swimming particles to accumulate near boundaries is the most noticeable characteristic of confined active suspensions. This was first discovered by Rothschild [6], who examined the distribution of swimming bull spermatozoa in a glass chamber and reported that there was a strong concentration peak close to the walls. When Berke et al. [7] carried out the same experiment again with Escherichia coli suspensions in microchannels, they also noticed a substantial accumulation of bacteria on the channel walls. They also mentioned how bacteria tended to align parallel to boundaries.

Hill et al. [8] conducted experiments tracking Escherichia coli trajectories near a rigid surface in a microfluidic channel, proposing a complex mechanism for their upstream swimming involving flagellar bundles chirality and hydrodynamic interactions. Subsequently, Kaya and Koser [9] further characterized their hydrodynamic interactions, showing that Escherichia coli cells undergo modified Jeffery orbits near walls [10]. Measuring and characterizing this hydrodynamic phenomenon has been a major objective of their work [9] as a first step in modeling and understanding shear-assisted orientation and upstream migration. Yet more recent research by Kaya and Koser [11], who methodically examined Escherichia coli motility near a surface as a function of the local shear rate, provided a clearer understanding of this phenomenon. They deduced that individual bacteria entering a flow system can rapidly migrate upstream. As previously explained by Lauga et al. [12], circular trajectories were seen at low shear rates because of the chirality of the cells. Positive rheotaxis was reported at higher shear rates, and it was accompanied by swift and continuous upstream motility. The combined effects of surface hydrodynamic interactions and orientation by the shear flow, which aligns the cells against the flow, were used to explain this directional swimming. The majority of confinement-based experimental studies have concentrated on swimming dynamics and near-wall aggregation. Secchi et al. [13] established that fluid flow predominantly governs the colonization of non-planar surfaces by motile bacteria. This was demonstrated through microfluidic experiments on Pseudomonas aeruginosa and Escherichia coli bacteria. Velocity gradients on curved surfaces dictate preferential attachment to specific regions. This is contrary to the case of nonmotile cells that attach at namely the leeward side of cylinders and immediately below apexes on corrugated surfaces [13]. Vennamneni et al. [14] investigated shear-induced migration of microswimmers in a dilute suspension.

They found that the steady state concentration profile is a function of the rotary Peclet number and the particle aspect ratio. Hernandez-Ortiz et al. [15, 16] performed direct numerical simulations of hydrodynamically interacting swimming particles contained in a gap between two plates using a straightforward dumbbell model. They found a strong particle accumulation at the boundaries in diluted systems. Elgeti and Gompper [17] introduced a Fokker-Planck description of active Brownian suspensions. They observed excellent agreement between analytical solutions and numerical results in simulations of self-propelled spheres in limits of narrow channels or small propulsion velocities despite completely ignoring hydrodynamic interactions. This study suggests that neither shape anisotropy nor wall hydrodynamic interactions are necessary to understand migration. Lee [18] proposed a comparable continuum model and derived analytical expressions for the ratio of particles in the bulk to those in the near-wall region for weak and strong rotational diffusion limits. Li and Ardekani [19] conducted direct numerical simulations of confined suspensions of spherical squirmers propelled by an imposed slip velocity, observing substantial accumulation at the boundaries irrespective of propulsion details. They also observed a tendency of particles to align perpendicularly to the wall in the near-wall region. Saintillan and Shelley [20, 21] introduced a class of models to elucidate the emergence of collective motion in semi-dilute suspensions. These models relie on a conservation equation for the distribution function representing particle positions and orientations. These models consider fluxes resulting from self-propulsion, advection, rotation by the background fluid flow, and diffusive processes. Baskaran and Marchetti [22] derived a continuum description of a suspension of active organisms that includes fluid-mediated, long-range hydrodynamic interactions among swimmers, showing that these interactions offer a straightforward, universal explanation for various nonequilibrium phenomena observed in the literature [23–27], independent of the microscopic physical model of individual swimmers. Forest et al. [28] developed a kinetic model for active polar liquid crystalline polymers, which exhibits a variety of excitable and stationary patterns in dilute regimes. Ezhilan and Saintillan [29] investigated the dynamics of confined suspensions of active particles subjected to pressure-driven flow using a kinetic model that incorporates detailed treatment of boundary conditions. They found peculiar dynamics, including wall accumulation, upstream swimming, centerline depletion, and shear-trapping, and provide analytical expressions for concentration and polarization profiles, demonstrating excellent agreement with numerical simulations and experimental observations.
In the previous numerical studies, the translational diffusion is addressed as an isotropic constant, while in fact the translational diffusion is anisotropic that depends on particle orientations. This work focuses on tackling the absence of consideration for anisotropic translational diffusion in previous numerical researches regarding the active particles. A numerical method based on the approach of Férec et al. [30] and Mezi et al. [1], utilizing the finite volume method, is updated, by changing the translational diffusion into an anisotropic tensor, to solve for the orientation of active Brownian particles. The extra stress contributions exerted by the active particles are not taken into consideration to clearly highlight the effect of the anisotropic diffusion on the suspensions.
The structure of this chapter is as follows. Sec. II focuses on the theoretical modeling. Then Sec. III describes the numerical model used to solve the active particle suspensions. Finally before the conclusion, Sec. IV shows the numerical results in two geometries, planar infinite channel then a planar channel with introducing a circular obstacle.

II. HYPOTHESIS

Consider a suspension of Brownian rodlike active particles of length L and width d. The active rods are monodispersed, neutrally buoyant, and rigid. The suspension is considered in the dilute concentration regime. Active rods are polar (the head of the rod is not identical to its tail). A position vector $\mathbf{r}_c$ and an orientation unit vector $\mathbf{p}$ describe each rod. For simplification, the extra stress contribution is not considered in this work.

A. Kinetic model equation

A suspension of active Brownian particles can be described via a probability distribution function $\Psi(\mathbf{r}_c, \mathbf{p}, t)$. It represents the probability to find particles at location $\mathbf{r}_c$ with orientation $\mathbf{p}$, at the instant t. In a dilute regime, a single-particle Smoluchowski equation can be obtained as

$$\frac{\partial \Psi}{\partial t} = -\nabla_{\mathbf{x}} \cdot (\dot{\mathbf{r}}_c \Psi) - \nabla_{\mathbf{p}} \cdot (\dot{\mathbf{p}} \Psi) \,. \tag{1}$$

The evolution of the position of an active Brownian particle with respect to time , $\dot{\mathbf{r}}_c$, is [21]

$$\dot{\mathbf{r}}_c = \mathbf{u} + V_s \mathbf{p} - \mathbf{D}_t \cdot \nabla_{\mathbf{x}} \log \Psi, \tag{2}$$

where V_s is the particle velocity. The evolution of its orientation with respect to time, $\dot{\mathbf{p}}$, can be written as

$$\dot{\mathbf{p}} = \dot{\mathbf{p}}_j - D_r \nabla_{\mathbf{p}} \log \Psi, \tag{3}$$

where $\dot{\mathbf{p}}_j$ is the Jeffery's equation and it is given by [10]

$$\dot{\mathbf{p}}_j = -\frac{1}{2}\boldsymbol{\omega} \cdot \mathbf{p} + \frac{\lambda}{2}\left(\dot{\boldsymbol{\gamma}} \cdot \mathbf{p} - \dot{\boldsymbol{\gamma}} : \mathbf{ppp}\right). \tag{4}$$

D_r and $\mathbf{D}_t$ are the rotary diffusion coefficient and translational diffusion tensor , respectively. The latter for non-spherical, rigid particles is defined by $\mathbf{D}_t = D_{\parallel}\mathbf{pp} + D_{\perp}(\boldsymbol{\delta} - \mathbf{pp})$, where $D_{\parallel}$ and $D_{\perp}$ are constants that characterize the diffusion parallel and perpendicular to the particle axis [31]. $\mathbf{u}$ is the external flow velocity vector at location $\mathbf{r}_c$. $\nabla_{\mathbf{p}}$ and $\nabla_{\mathbf{x}}$ denote the gradient operators in configurational and spatial spaces, respectively. $\boldsymbol{\omega}$, $\dot{\boldsymbol{\gamma}}$, and $\boldsymbol{\delta}$ are the vorticity, strain rate, and identity tensors, respectively. λ is a constant form factor as a function of the particle aspect ratio $a_r = L/d$, in the case of rods, $\lambda = 1$. Hence, the expanded version of Eq. 1, by taking into account the fluid incompressibility condition, is

$$\frac{D\Psi}{Dt} = -\nabla_{\mathbf{x}} \cdot (V_s \mathbf{p}\Psi) + \nabla_{\mathbf{x}} \cdot (\mathbf{D}_t \cdot \nabla_{\mathbf{x}}\Psi) - \nabla_{\mathbf{p}} \cdot (\dot{\mathbf{p}}_j \Psi) + D_r \nabla^2_{\mathbf{p}}\Psi, \tag{5}$$

where $\frac{D(...)}{Dt} = \frac{\partial(...)}{\partial t} + \mathbf{u} \cdot \nabla_{\mathbf{x}}(...)$ is the material derivative operator, and $\nabla^2_{\mathbf{p}}$ is the Laplacian operator in configurational domain.

B. Flow problem

The problem is governed by the Stokes equations in the limit of creeping flow

$$\nabla_{\mathbf{x}} \cdot \mathbf{u} = 0, \tag{6}$$

$$-\eta_0 \nabla^2_{\mathbf{x}}\mathbf{u} + \nabla_{\mathbf{x}} P = \mathbf{0}. \tag{7}$$

In the above equations, $\nabla^2_{\mathbf{x}}$ is the Laplacian operator in the spatial space, η_0 is the dynamic viscosity of the Newtonian suspending fluid, P denotes the pressure. The extra stress contribution by the particles and brownian motion is set to zero for simplicity and in order to highlight the effect of the translational diffusion.

C. Dimensionless formulation of the problem

Choosing the active rod length L as the characteristic length and the characteristic strain rate $\dot{\gamma} = U_{avg}/L$, where U_{avg} is the average flow velocity, and the dimensionless concentration $c^* = \frac{c}{n}$, where n is the mean number density. The dimensionless form of FP equation (Eq. 5) is

$$\frac{D\Psi}{D\tau} = -Pe_s \nabla^*_{\mathbf{x}} \cdot (\mathbf{p}\Psi) + \nabla^*_{\mathbf{x}} \cdot \left\{ \left[\frac{1}{Pe_{\parallel}}\mathbf{pp} + \frac{1}{Pe_{\perp}}(\boldsymbol{\delta} - \mathbf{pp}) \right] \cdot \nabla^*_{\mathbf{x}}\Psi \right\} - \nabla_{\mathbf{p}} \cdot (\dot{\mathbf{p}}_j \Psi) + \frac{1}{Pe_r}\nabla^2_{\mathbf{p}}\Psi, \tag{8}$$

where $Pe_s = \frac{V_s}{L\dot{\gamma}}$ is a dimensionless number that represents the relative velocity of the active rod with respect to the flow velocity. This dimensionless number can provide insights into how active rods respond to the applied shear flow. For example, if Pe_s is much smaller than 1, it suggests that the active rod moves relatively slowly compared to the rate of deformation, indicating a less responsive or less mobile active rod. Conversely, if Pe_s is close to or greater than 1, it suggests that the active rod moves more rapidly in comparison to the flow velocity, indicating a more mobile or responsive active rod. The dimensionless equation of flow is

$$-\nabla^{*2}_{\mathbf{x}}\mathbf{u}^* + \nabla^*_{\mathbf{x}} P^* = \mathbf{0} \tag{9}$$

III. NUMERICAL MODEL

This study focuses on a 2D problem confining the active rod on a plane with one configurational coordinate (θ), and two spatial Cartesian coordinates x and y. At each spatial node, this multidimensional problem imposes a mesh for the active rod orientation angle θ domain. The partial differential equation, Eq. 8, is discretized in the configurational space using the finite volume technique (FVM). The FVM is known for having the local conservativeness property required to satisfy the model formalized normalization constraint for the PDF. Following the work of Férec et al. [30] and Mezi et al. [1] the model is updated to solve Eq. 8 for active rods with an anisotropic diffusion tensor. In this context, all the possible orientations describe a full circle of unit radius since an active rod is polar. As a result, the perimeter of the circle has been divided into N equal intervals of length $\Delta\theta = 2\pi/N$. The convection-diffusion problem is solved using an upwinding power-law approach in the configurational space [32]. Therefore, the descritized form for nodal points P, E and W of the FP equation, Eq. 8, is

$$\Delta\theta\frac{\partial\Psi_p}{\partial\tau} + \Delta\theta\mathbf{u}\cdot\nabla_{\mathbf{x}}\Psi_p - \Delta\theta\nabla_{\mathbf{x}}\cdot\left\{\left[\frac{1}{Pe_\perp}(\mathbf{pp}+\boldsymbol{\delta})\right]\cdot\nabla_{\mathbf{x}}\Psi_p\right\} + \Delta\theta Pe_s\nabla_{\mathbf{x}}\cdot\Psi_p + a_P\Psi_P - a_W\Psi_W - a_E\Psi_E = 0. \quad (10)$$

COMSOL Multiphysics 6.1 is used, which enables coupling of the existing laminar flow interface with partial differential equation (PDE) interfaces, which are necessary for simulating the additional active rod stresses, the whole problem (i.e., flow field and fiber orientation) is solved using this software with livelink with MATLAB R2022B to implement the equations. Given that there are NxN nodal points involved in discretization of Ψ, the coupled system of PDEs is represented by using the matrix coefficient forms.

IV. NUMERICAL RESULTS

We employ the Finite Volume method to investigate two flow problems, solving the problem defined in Eqs. 6, 7 and 10. The indices 1 and 2 represent the flow direction and the velocity gradient direction, respectively. In a simple shear flow and Poiseuille flow, they indicate x and y, respectively.

A. Poiseuille flow

We conduct simulations within a square 2D channel with a side length of H, featuring a Poiseuille flow between two stationary walls defined by $(U/(\dot{\gamma}H)) = 1-4(y/H)^2)$. To simulate an infinitely long channel, periodic flow conditions are employed with a constant flow rate (as depicted in Fig. 1). The initial conditions are set to $\Psi = 1/2\pi$, where active rods are assumed to be initially random planar and homogeneously distributed along the channel. This means that the initial conformation tensor conditions are set as $A_{ii} = 1/3$ and $A_{ij} = 0$ for $i \neq j$.

1. Effect of particles velocity

Based on the diffusion Peclet numbers (Pe_r and $Pe_\perp$) and the active rod self-propulsion Peclet numbers (Pe_s), we investigate three different regimes. The first regime ($Pe_s = 0, Pe_r, Pe_\perp$) investigates conditions in which the directed motion resulting from self-propulsion is only marginally present. The second regime ($Pe_s = Pe_r = Pe_\perp$) corresponds to situations in which active motion and diffusion are in competition. The third regime ($Pe_s > Pe_r, Pe_\perp$) examines circumstances in which active motion takes precedence over diffusion. In this instance, $Pe_\perp = Pe_r = 10$ and $Pe_s = 0, 5, 10$, and 15 are the fixed Peclet numbers. No extra stress caused by active rods is taken into account, and the flow issue is derived from Eq. 9. The concentration profiles, as depicted in Figure 2a, shows active rod accumulation near the walls. This is particularly evident at higher values of the self-propulsion Peclet number (Pe_s). This accumulation of active rods near the walls is accompanied by a decrease in their alignment in the flow direction, as indicated in Fig. 2b. In practice, as a result of this buildup near the walls, the concentration regimes may shift towards semi-concentrated or concentrated. However, for the sake of simplicity, we are disregarding these changes in concentration regimes. Moreover, the nematic order parameter, as shown in Figs. 2c and 2d, indicates a higher nematic alignment near the walls. In this context, the nematic director n_2 shares the same direction as the wall-normal coordinate y and exhibits a substantially higher absolute value near the walls, gradually diminishing towards the center of the channel.

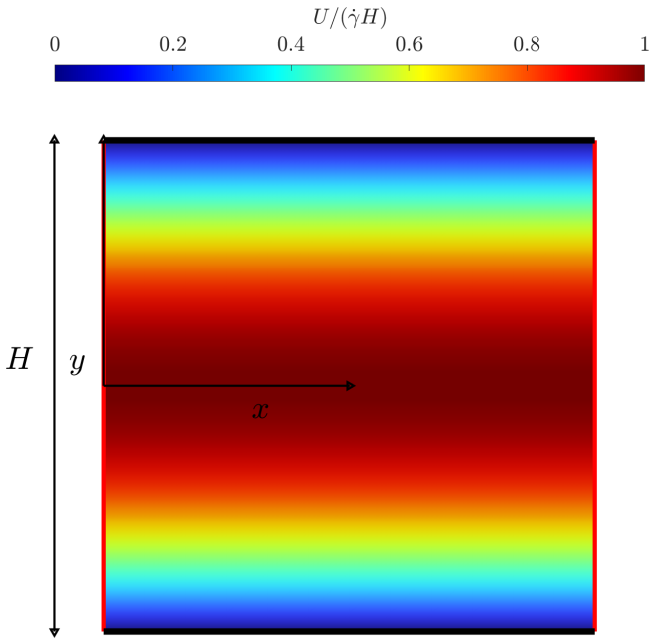

FIG. 1: Dimensionless velocity magnitude in the squared channel, of side H, for Poiseuille flow with periodic BC. The vertical red lines represent the periodic conditions.

Fig. 2b provides insight into the alignment of active rods along the y-direction at steady state. Increasing the self-propulsion (Pe_s) results in a more alignment of the active rods in the direction of the flow. This alignment phenomenon arises due to the interplay between self-propulsion and fluid flow-induced shear. As the active rods exhibit stronger self-propelled motion with higher Pe_s, this active motion enhances the rod orientations induced by the flow in the flow direction, with higher alignment around the center of the channel. This alignment effect is particularly pronounced due to the dominance of self-propulsion over diffusion, leading to organized patterns of alignment parallel to the flow direction.

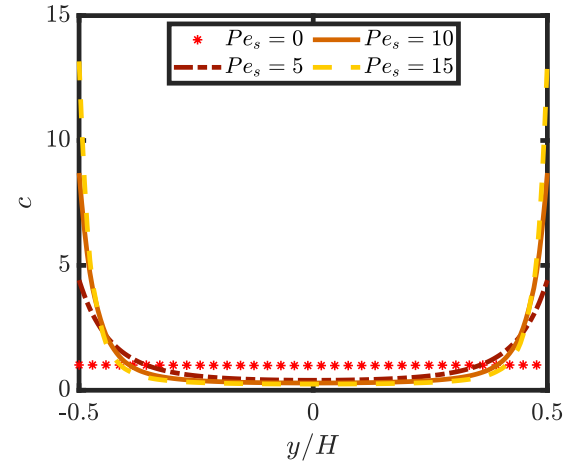

(a) Effect of the particles self-propulsion Peclet number, Pe_s, on the concentration distribution, c, along the y direction.

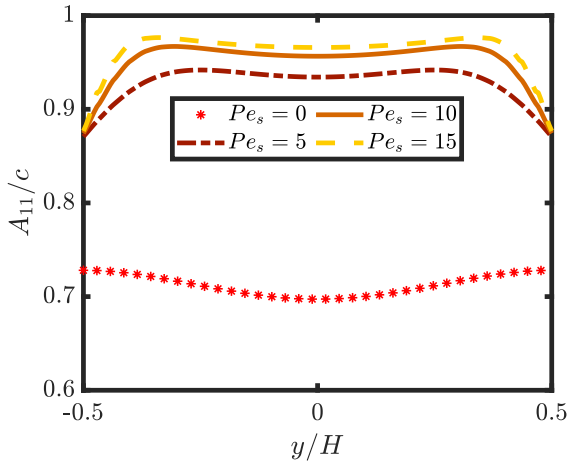

(b) Effect of the particles self-propulsion Peclet number, Pe_s, on the orientation component, A_{11}/c, along the y direction.

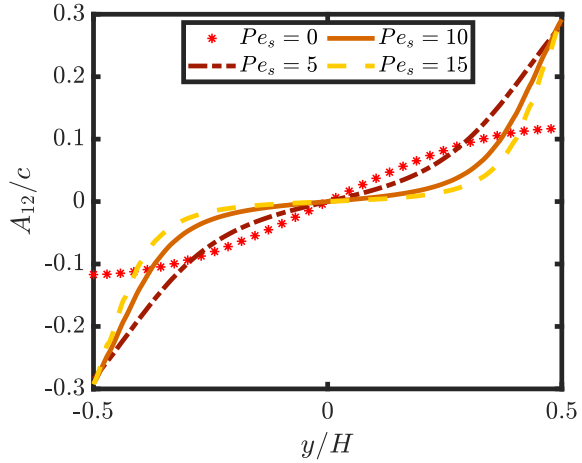

(c) Effect of the particles self-propulsion Peclet number, Pe_s, on the orientation component, A_{12}/c, along the y direction.

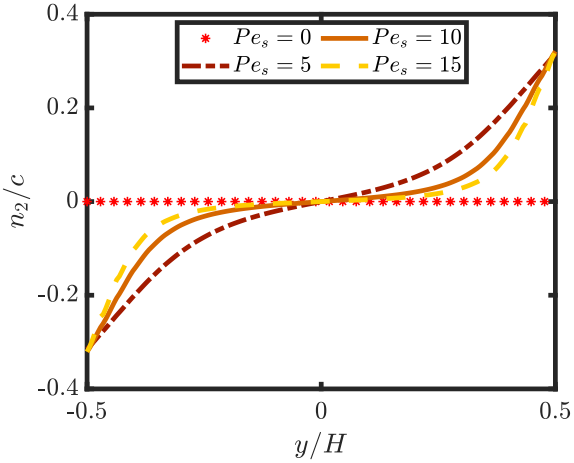

(d) Effect of the particles self-propulsion Peclet number, Pe_s, on the nematic order, n_2/c, along the y direction.

FIG. 2: Showing the effect of the particles self-propulsion Peclet number, $Pe_s = 0, 5, 10$ and 15, (a) on the concentration distribution, c, (b) on the orientation component, A_{11}/c, (c) on the orientation component, A_{12}/c, (d) on the nematic order, n_2/c, along the y direction at steady state, in Poiseuille flow.

2. *Effect of anisotropic translational diffusion*

Here, we want to understand how directional diffusion affects the suspension active rods as opposed to the isotropic translational diffusion. We fixed the particles self-propulsion Peclet number $Pe_s = 5$ and the rotary Peclet number $Pe_r = 10$. We compare a constant translational Peclet number (replacing the diffusion tensor in Eq. 8) $Pe = \frac{Pe_{\parallel}+Pe_{\perp}}{2}$ ($Pe_{\perp} = 10$), with the case when the translational diffusion is a tensor.

In the case of anisotropic translational diffusion, the active rods experience various effective diffusions depending on their orientations. Figs. 3a and 3b show the concentration results examining an isotropic translational diffusion and an anisotropic translational diffusion, respectively. Both cases predict the migration of active rods toward the fixed walls. Fig. 3b shows strong accumulation of active rods at the wall, while Fig. 3a shows a moderate migration. Anisotropic diffusion can also influence the alignment behavior of the active rods. Figs. 4a and 4b show the orientation of the active rods in the flow direction (x direction). The directional dependence of diffusion contributes to a more pronounced alignment of active rods with the flow direction. In the case of isotropic diffusion, the active rods experience the same diffusion coefficient in all directions, resulting in a more uniform and isotropic exploration of the flow field. While

the active rods can still migrate towards low shear regions and align with the flow direction, the isotropic nature of diffusion limits the migration enhancement compared to the anisotropic case. The isotropic diffusion leads to a more moderate alignment of active rods the flow direction, and the migration towards low shear regions is less pronounced compared to the anisotropic case.

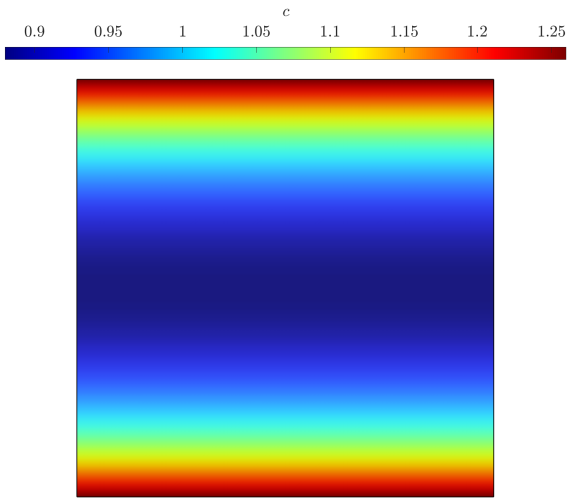

(a) Concentration distribution c at steady state for isotropic traslational diffusion.

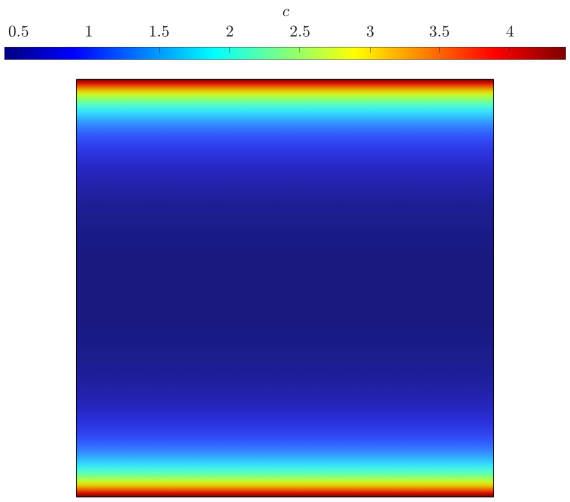

(b) Concentration distribution c at steady state for anisotropic translational diffusion.

FIG. 3: Showing the effect of (a) isotropic translational diffusion and (b) anisotropic translational diffusion on the concentration distribution c along the channel at steady state.

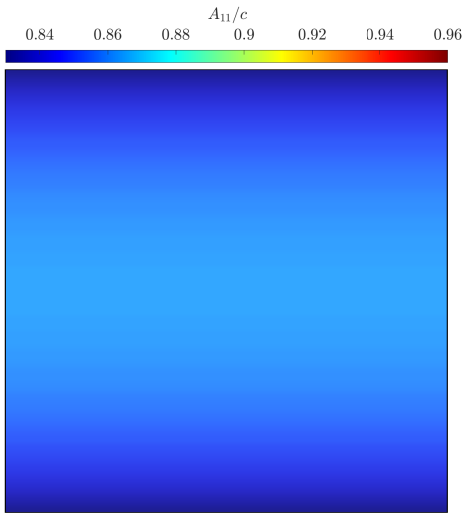

(a) Orientation component distribution A_{11}/c at steady state for isotropic translational diffusion.

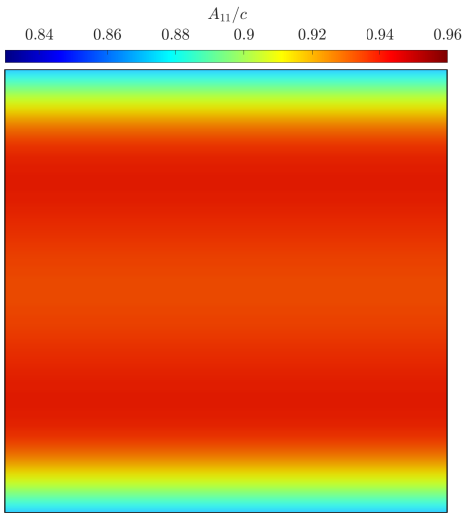

(b) Orientation component distribution A_{11}/c at steady state for anisotropic translational diffusion.

FIG. 4: Showing the effect of (a) isotropic translational diffusion and (b) anisotropic translational diffusion on the orientation component A_{11}/c along the channel at steady state.

3. *Effect of rotary diffusion*

We conducted simulations to explore the effects of varying rotary Peclet numbers (Pe_r), focusing on cases where Pe_r values were set at $1, 10, 100$, and 1000. To maintain consistency, we kept the particle self-propulsion Peclet number is fixed at $Pe_s = 5$, and the translational diffusion coefficient was maintained at a constant value represented by $Pe_\perp = 10$. As anticipated, the outcomes revealed that higher rotary Peclet numbers tend to attenuate the alignment of active rods in the direction of the flow. Moreover, our investigations unveiled an intriguing trend: increasing in Pe_r led to higher active rod accumulation toward the channel walls (see Fig. 5a). This trend mirrors the behavior observed in passive rod systems, where the migration of actively aligned rods becomes less prominent as the value of Pe_r increases. Additionally, Fig. 5b indicates that the nematic order of active rods near the walls is influenced by rotary diffusion. Notably, as the rotary Peclet number (Pe_r) decreases, the nematic order exhibits a discernible increase. This finding suggests that the interaction between rotary diffusion and the fluid dynamics plays a crucial role in shaping the spatial distribution and alignment of active rods in the channel. These results are in good agreement with the work of Matilla et al. [33], where the increase of the rotary Peclet number leads to more accumulations at the walls.

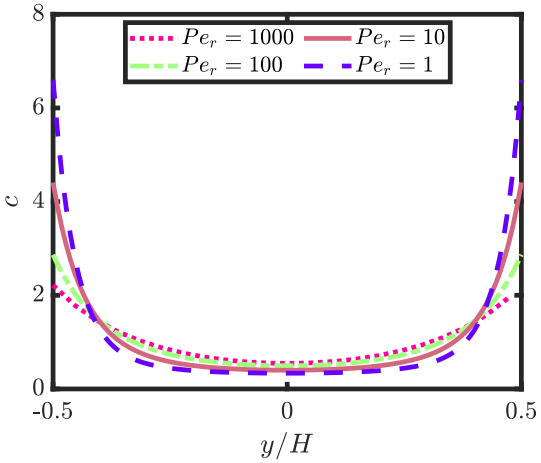

(a) Effect of the rotary diffusion, Pe_r, on the concentration distribution, c, along the y direction.

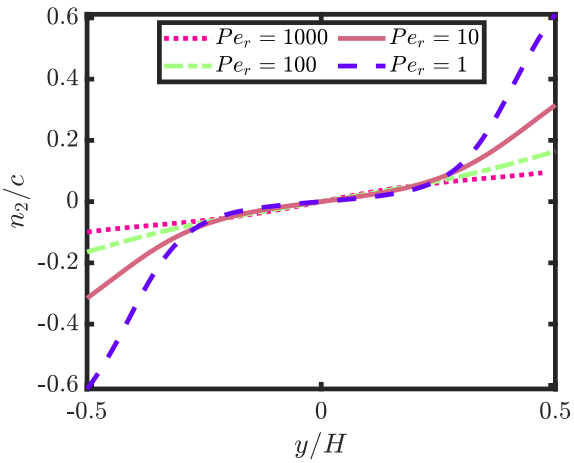

(b) Effect of the rotary diffusion, Pe_r, on the nematic order, n_2/c, along the y direction.

FIG. 5: Showing the effect of the rotary diffusion, $Pe_r = 1, 10, 100$ and 1000, (a) on the concentration distribution, c, (b) on the nematic order, n_2/c, along the y direction at steady state, in Poiseuille flow.

4. *Effect of translational diffusion*

In the context of parabolic flow, we are investigating the influence of translational diffusion on a system of active rods. To examine this, we maintained a constant particles self-propulsion Peclet number of $Pe_s = 5$ and a rotary diffusion coefficient of $Pe_r = 10$, while systematically varying the translational Peclet number with different values, $Pe_\perp = 0.1, 1$, and 10. Our findings illustrate that at higher $Pe_\perp$ values, active rods tend to accumulate near the channel walls. Conversely, as $Pe_\perp$ decreases, this wall accumulation tendency diminishes, eventually resulting in a more uniform distribution of active rods along the channel. Notably, when $Pe_\perp = 0.1$, active rods exhibit a nearly homogeneous distribution throughout the channel.

Fig. 6b shows that under higher $Pe_\perp$ conditions, active rods exhibit a heightened orientation preference aligned with the flow direction. In contrast, lower $Pe_\perp$ values coincide with active rod orientations that approach a more randomized distribution. This observation implies that the translational Peclet number acts as a constraining factor on the self-propulsion dynamics of active rods. Figs. 6c and 6d reveal that the quantity A_{12}/c exhibits the same direction in comparison to y/H, and n_2/c aligns with the same direction as y/H. This alignment pattern suggests that the active rods exhibit polarization towards the flow direction, accompanied by nematic order directed towards the walls of the channel.

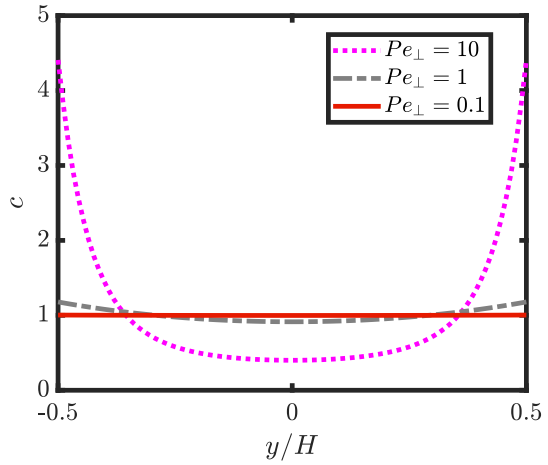

(a) Effect of the particles self-propulsion Peclet number, Pe_s, on the concentration distribution, c, along the y direction.

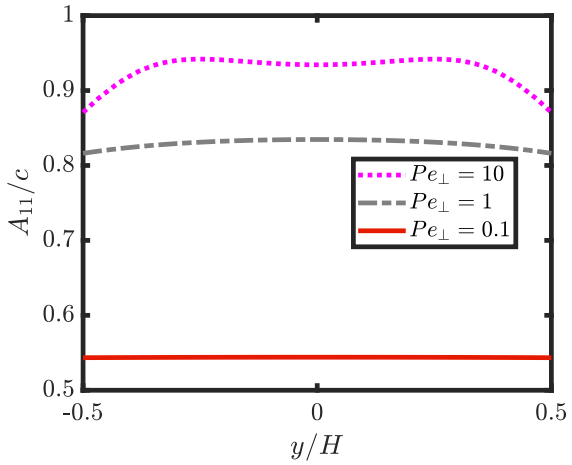

(b) Effect of the particles self-propulsion Peclet number, Pe_s, on the orientation component, A_{11}/c, along the y direction.

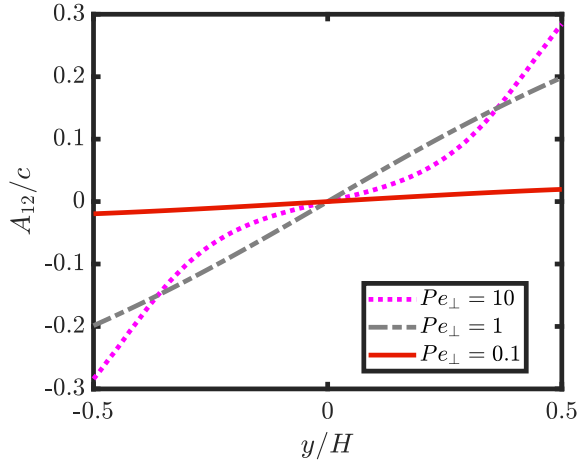

(c) Effect of the particles self-propulsion Peclet number, Pe_s, on the orientation component, A_{12}/c, along the y direction.

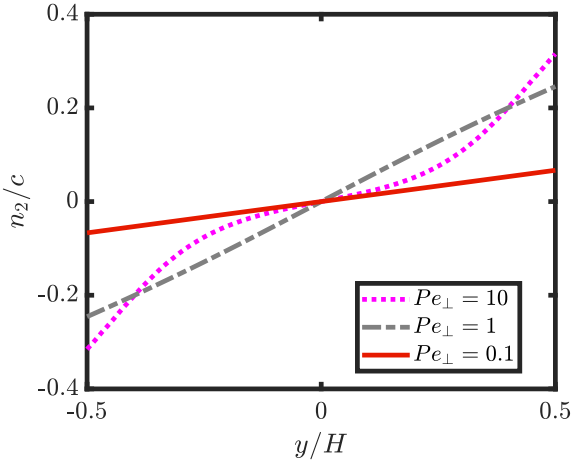

(d) Effect of the particles self-propulsion Peclet number, Pe_s, on the nematic order, n_2/c, along the y direction.

FIG. 6: Showing the effect of the translational diffusion, $Pe_\perp = 0.1, 1$ and 10, (a) on the concentration distribution, c, (b) on the orientation component, A_{11}/c, (c) on the orientation component, A_{11}/c, (d) the nematic order, n_2/c, along the y direction at steady state, in Poisseuille flow.

B. Results of flow with a circular obstacle

To thoroughly validate and extend the applicability of this model [34, 35], it is imperative to assess its performance in the context of active rods. This step will contribute significantly to enhancing our understanding of how active rods navigate through complex environments, shedding light on their behavior in real-world situations.Indeed, incorporating a model that captures the interaction between suspended rods and obstacles is crucial for comprehending the dynamics of particulate suspensions in diverse engineering scenarios. In fact, biofilms formation on various things, including industrial and maritime infrastructure, can be a serious issue. The prevention methods can indeed be costly [36], and researchers are continuously exploring ways to address this issue more efficiently and economically [37, 38]. Spoting the biofilms formation areas can help in solving the problems. The study is conducted within a planar channel characterized by a width of $2H$ and a length of $W = 3H$. To introduce complexity, a circular obstacle with a radius of $R = 0.5H$ is placed at the center of the channel ($x = H$) as depicted in Fig. 7. This work is performed by Issa et al. [39] for passive rods. The study is conducted for $Pe_r = Pe_\perp = 10$.

In the context of a Poiseuille flow channel with the inclusion of a circular obstacle, we have investigated the distribution

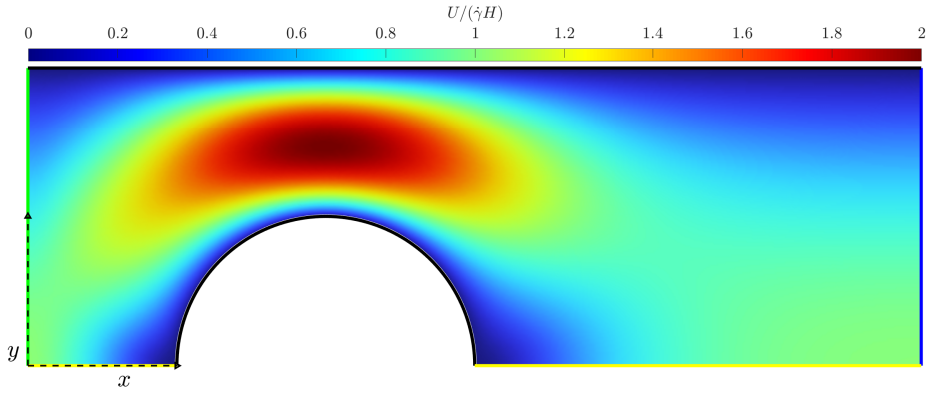

FIG. 7: Dimensionless velocity magnitude a rectangular channel, for the precence of circular obstacle. The vertical green line represents the inlet, the horizontal yellow line represents the symmetric and the vertical blue line represents the outlet.

of active rod concentration. The concentration profile, as depicted in Fig. 8a, underscores intriguing spatial variations. Specifically, active rods exhibit heightened concentration both near the channel walls and preceding the obstacle. However, there is a substantial decline in active rod concentration downstream of the obstacle. Interestingly, the behavior becomes more pronuanced as the self-propulsion (Pe_s) of the active rods increases. In particular, with elevated Pe_s, active rods tend to accumulate more prominently along the channel walls and in the region preceding the obstacle. This zone of accumulation becomes narrower with higher active rod concentration. Moreover, Fig. 8b sheds light on the orientation of active rods. Specifically, active rods are observed to align in the x direction at the rear of the obstacle and in the upper part of the channel. Conversely, before and after the obstacle, particularly at the center of the channel ($y = 0$), active rods adopt an orientation opposite to the flow direction. As shown in the study, biofilms are formed at the rear part of the obstacle. These findings are in quantative agreement with the work of Mino et al. [40] were they found accumulation of motile bacteria at the rear of a confined obstacle.

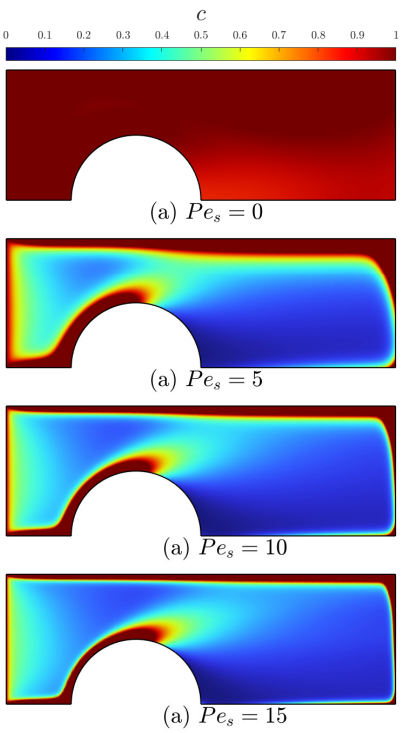

(a) $Pe_s = 0$

(a) $Pe_s = 5$

(a) $Pe_s = 10$

(a) $Pe_s = 15$

(a) Effect of the particles self-propulsion Peclet number, Pe_s, on the concentration distributon, c, along the channel, at steady state.

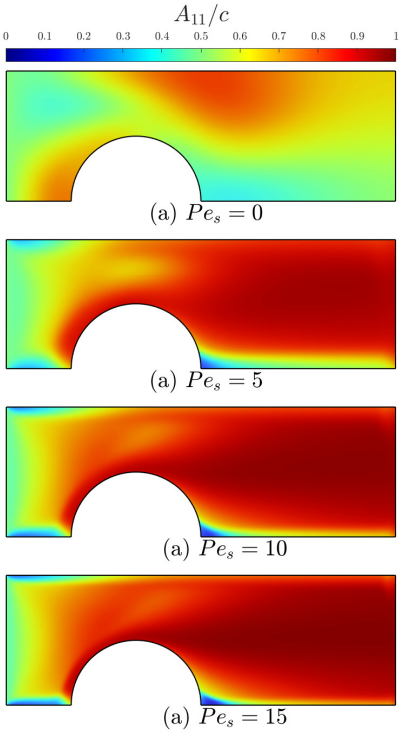

(a) $Pe_s = 0$

(a) $Pe_s = 5$

(a) $Pe_s = 10$

(a) $Pe_s = 15$

(b) Effect of the particles self-propulsion Peclet number, Pe_s, on the orientation component, A_{11}/c, along the channel, at steady state.

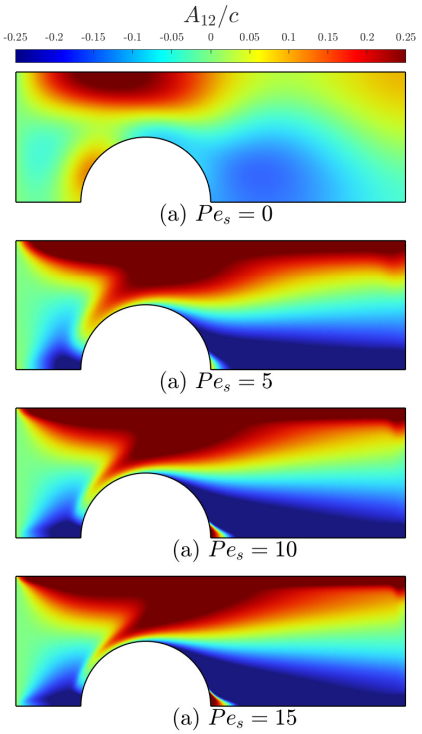

(a) $Pe_s = 0$

(a) $Pe_s = 5$

(a) $Pe_s = 10$

(a) $Pe_s = 15$

(c) Effect of the particles self-propulsion Peclet number, Pe_s, on the orientation component, A_{12}/c, along the channel, at steady state.

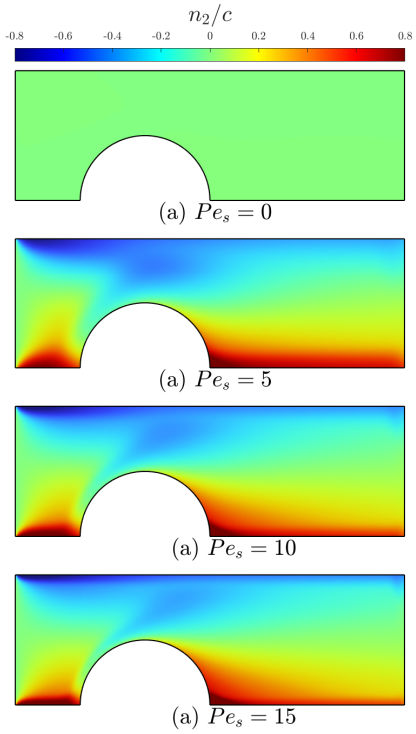

(a) $Pe_s = 0$

(a) $Pe_s = 5$

(a) $Pe_s = 10$

(a) $Pe_s = 15$

(d) Effect of the particles self-propulsion Peclet number, Pe_s, on the nematic order, n_2/c, along the channel, at steady state.

FIG. 8: Showing the effect of the particles self-propulsion Peclet number, $Pe_s = 0, 5, 10$ and 15, with the presence of a circular obstacle on (a) the concentration distribution, c, (b) the orientation component, A_{11}/c, (c) the orientation component, A_{12}/c, (d) the nematic order,n_2/c, at steady state.

Fig. 8c and Fig. 8d provide insights into the orientation characteristics of the active rods within the channel containing a circular obstacle. Specifically, Fig. 8c depicts the values of the orientation component A_{12}/c, while Fig. 8d illustrates the nematic order n_2/c. In the upper region of the obstacle, extending to the walls, both A_{12}/c and n_2/c exhibit positive values. This indicates that active rods are polarized in the positive x direction and oriented towards the wall. Conversely, at the center of the channel, both A_{12}/c and n_2/c take on negative values. This implies that active rods in this region are polarized in the positive x direction but oriented towards the channel's center.
A distinct behavior is observed immediately after the obstacle in a small area at the center. Here, A_{12}/c remains positive while n_2/c takes on a negative value. This signifies that active rods are polarized in the negative x direction and oriented towards the channel's center in this specific region.

V. CONCLUSION

In conclusion, this work explores the behavior of active rod suspensions in different flow systems, Poiseuille flow in infinite channels, and introducing a circular obstacle in channel with Poiseuille flow at the inlet. The study examines the dynamics of active rods including active rod migrations, orientations and the nematic order through a numerical simulations based on the volume method with taking into consideration an anisotropic translational diffusion.
The active rods favor the accumulation at the walls of the channel, in addition active rods are more aligned in the flow direction than the passive rods. Although, randomly aligned active rods at low rotary Peclet numbers Pe_r have more tendency to migrate toward the walls than the aligned active rods. It is shown that translational diffusion hinders the effect of the active rods and at low translational Peclet numbers $Pe_\perp$, the system returns to act as the case of the passive rods. When a circular obstacle is presented, active rods are accumulated at the walls and at the back of obstacle for active rods, while after the obstacle, they are more aligned in the inlet flow direction (x direction) except in the center of the channel, they are aligned in the velocity gradient direction y direction.
To confirm and build upon these findings, additional study and experimentation are required. Future work will focus in expanding this work to 3D. In addition of developing a good closure approximation for the kinetic model that can predict the orientation, concentration and the rheological properties of the active rods with less computational effort.

Appendix A: Second-order moment of Ψ

The second-order moment of Ψ, $\mathbf{A}_2$, contains information on the local concentration and orientation of particles and is defined as

$$\mathbf{A}_2 = \int_{\mathbf{p}} \mathbf{pp}\Psi d\mathbf{p}, \tag{A1}$$

The trace of $\mathbf{A}_2$ is the concentration field c, which represents the mean number density in the suspension, it is the zeroth-order moment of Ψ

$$c = \mathbf{A}_2 : \boldsymbol{\delta} = \int_{\mathbf{p}} \Psi d\mathbf{p}, \tag{A2}$$

The first order moment of Ψ, $\mathbf{n}$, represents the nematic order of the particles and it is defined as

$$\mathbf{n} = \int_{\mathbf{p}} \mathbf{p}\Psi d\mathbf{p}, \tag{A3}$$

The third-order moment of Ψ, $\mathbf{A}_3$, is defined as

$$\mathbf{A}_3 = \int_{\mathbf{p}} \mathbf{ppp}\Psi d\mathbf{p}, \tag{A4}$$

while the fourth-order moment of Ψ, $\mathbf{A}_4$, is defined as

$$\mathbf{A}_4 = \int_{\mathbf{p}} \mathbf{pppp}\Psi d\mathbf{p}, \tag{A5}$$

The evolution equation of the concentration of the active particles in a suspending fluid is

$$\frac{Dc}{Dt} = D_\perp \nabla^2_{\mathbf{x}} c + (D_\parallel - D_\perp)\nabla_{\mathbf{x}}\nabla_{\mathbf{x}}\mathbf{A}_2 + V_s \nabla_{\mathbf{x}} \cdot (c\mathbf{n}) \tag{A6}$$

V represents the volume, which is large enough to contain a statistically significant number of particles but smaller than the characteristic length scale of the macroscopic properties of the system under consideration. In the case of active particles, the odd-order tensors do not equal zeros due to the non-symmetric shapes of the particles. Since the active particles are not symmetric, unlike the passive particles, the orientation component A_{12}/c is not enough to give information about the polarisation of the particle. Fig. 9 shows the different polarisation of the particle depending on the signs of A_{12} and n_2.

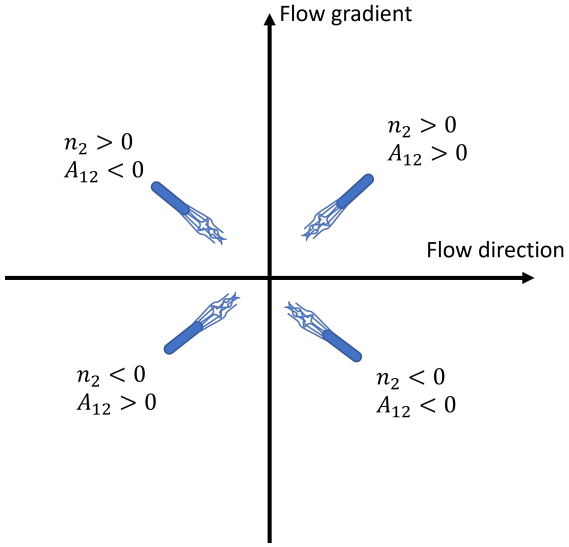

FIG. 9: Representation shows the meaning of the nematic order of a asymmetric particle.

The evolution of $\mathbf{A}_2$ is obtained by premultiplying Eq. **??** with the tensor $\mathbf{pp}/V$ and integrating it over the spatial and configurational spaces.

$$\begin{aligned}\frac{D\mathbf{A}_2}{Dt} =& -\frac{1}{2}\left(\boldsymbol{\omega}\cdot\mathbf{A}_2 - \mathbf{A}_2\cdot\boldsymbol{\omega}\right) + \frac{\lambda}{2}\left(\dot{\boldsymbol{\gamma}}\cdot\mathbf{A}_2 + \mathbf{A}_2\cdot\dot{\boldsymbol{\gamma}} - 2\mathbf{A}_4 : \dot{\boldsymbol{\gamma}}\right) \\ &+ 2D_r\left(c\boldsymbol{\delta} - \alpha\mathbf{A}_2\right) + D_\perp\nabla^2_{\mathbf{x}}\mathbf{A}_2 + \left(D_\parallel - D_\perp\right)\nabla_{\mathbf{x}}\nabla_{\mathbf{x}} : \mathbf{A}_4 + V_s\nabla_{\mathbf{x}}\cdot\mathbf{A}_3.\end{aligned} \tag{A7}$$

α equals 2 in 2D and 3 in 3D. It can be noticed that the time evolution of the tensor $\mathbf{A}_2$ depends on higher-order moments of Ψ. Hence, the problem requires a closure approximation. The last term in Eq. A7 is the Hessian operator and the last two terms of Eq. A7 implicitly show the coupling between the local concentration and the local orientation of Brownian particles. Unfortunately, unlike the case of passive particles, the closure approximations found in the literature do not work for non-symmetric particles. So the problem here requires closure approximations for solving $\mathbf{A}_4$ and $\mathbf{A}_3$ as a function of $\mathbf{A}_2$.

The derived macro-model enables one to solve a set of partial differential equations (PDEs) rather than a full 6D Fokker-Planck equation (Eq. **??**), to be discussed below, simplifying drastically the problem.

[1] D. Mezi, G. Ausias, S. G. Advani, and J. Férec, Fiber suspension in 2d nonhomogeneous flow: The effects of flow/fiber coupling for newtonian and power-law suspending fluids, Journal of Rheology **63**, 405 (2019).
[2] D. Woolley, Motility of spermatozoa at surfaces, REPRODUCTION-CAMBRIDGE- **126**, 259 (2003).
[3] S. Lecuyer, R. Rusconi, Y. Shen, A. Forsyth, H. Vlamakis, R. Kolter, and H. A. Stone, Shear stress increases the residence time of adhesion of pseudomonas aeruginosa, Biophysical journal **100**, 341 (2011).
[4] L. Lu and W. A. Walker, Pathologic and physiologic interactions of bacteria with the gastrointestinal epithelium, The American journal of clinical nutrition **73**, 1124S (2001).
[5] J. P. Celli, B. S. Turner, N. H. Afdhal, S. Keates, I. Ghiran, C. P. Kelly, R. H. Ewoldt, G. H. McKinley, P. So, S. Erramilli, *et al.*, Helicobacter pylori moves through mucus by reducing mucin viscoelasticity, Proceedings of the National Academy of Sciences **106**, 14321 (2009).
[6] ROTHSCHILD, Non-random distribution of bull spermatozoa in a drop of sperm suspension, Nature **198**, 1221 (1963).

[7] A. P. Berke, L. Turner, H. C. Berg, and E. Lauga, Hydrodynamic attraction of swimming microorganisms by surfaces, Physical Review Letters **101**, 038102 (2008).

[8] J. Hill, O. Kalkanci, J. L. McMurry, and H. Koser, Hydrodynamic surface interactions enable escherichia coli to seek efficient routes to swim upstream, Physical review letters **98**, 068101 (2007).

[9] T. Kaya and H. Koser, Characterization of hydrodynamic surface interactions of escherichia coli cell bodies in shear flow, Physical review letters **103**, 138103 (2009).

[10] G. B. Jeffery, The motion of ellipsoidal particles immersed in a viscous fluid, Proceedings of the Royal Society of London. Series A, Containing papers of a mathematical and physical character **102**, 161 (1922).

[11] T. Kaya and H. Koser, Direct upstream motility in escherichia coli, Biophysical journal **102**, 1514 (2012).

[12] E. Lauga, W. R. DiLuzio, G. M. Whitesides, and H. A. Stone, Swimming in circles: motion of bacteria near solid boundaries, Biophysical journal **90**, 400 (2006).

[13] E. Secchi, A. Vitale, G. L. Miño, V. Kantsler, L. Eberl, R. Rusconi, and R. Stocker, The effect of flow on swimming bacteria controls the initial colonization of curved surfaces, Nature communications **11**, 2851 (2020).

[14] L. Vennamneni, S. Nambiar, and G. Subramanian, Shear-induced migration of microswimmers in pressure-driven channel flow, Journal of Fluid Mechanics **890**, A15 (2020).

[15] J. P. Hernandez-Ortiz, C. G. Stoltz, and M. D. Graham, Transport and collective dynamics in suspensions of confined swimming particles, Physical review letters **95**, 204501 (2005).

[16] J. P. Hernandez-Ortiz, P. T. Underhill, and M. D. Graham, Dynamics of confined suspensions of swimming particles, Journal of Physics: Condensed Matter **21**, 204107 (2009).

[17] J. Elgeti and G. Gompper, Wall accumulation of self-propelled spheres, Europhysics Letters **101**, 48003 (2013).

[18] C. F. Lee, Active particles under confinement: aggregation at the wall and gradient formation inside a channel, New Journal of Physics **15**, 055007 (2013).

[19] G.-J. Li and A. M. Ardekani, Hydrodynamic interaction of microswimmers near a wall, Physical Review E **90**, 013010 (2014).

[20] D. Saintillan and M. J. Shelley, Instabilities, pattern formation, and mixing in active suspensions, Physics of Fluids **20** (2008).

[21] D. Saintillan and M. J. Shelley, Instabilities and pattern formation in active particle suspensions: kinetic theory and continuum simulations, Physical Review Letters **100**, 178103 (2008).

[22] A. Baskaran and M. C. Marchetti, Statistical mechanics and hydrodynamics of bacterial suspensions, Proceedings of the National Academy of Sciences **106**, 15567 (2009).

[23] C. Dombrowski, L. Cisneros, L. Chatkaew, R. Goldstein, and J. Kessler, Self-concentration and large-scale coherence in bacterial dynamics, Physical Review Letters **93**, 098103 (2004).

[24] O. A. Igoshin, R. Welch, D. Kaiser, and G. Oster, Waves and aggregation patterns in myxobacteria, Proceedings of the National Academy of Sciences **101**, 4256 (2004).

[25] I. H. Riedel, K. Kruse, and J. Howard, A self-organized vortex array of hydrodynamically entrained sperm cells, Science **309**, 300 (2005).

[26] F. J. Nedelec, T. Surrey, A. C. Maggs, and S. Leibler, Self-organization of microtubules and motors, Nature **389**, 305 (1997).

[27] V. Narayanan, S. Ramaswamy, and N. Menon, Long-lived giant number fluctuations in a swarming granular nematic, Science **317**, 105 (2007).

[28] M. G. Forest, Q. Wang, and R. Zhou, Kinetic theory and simulations of active polar liquid crystalline polymers, Soft Matter **9**, 5207 (2013).

[29] B. Ezhilan and D. Saintillan, Transport of a dilute active suspension in pressure-driven channel flow, Journal of Fluid Mechanics **777**, 482 (2015).

[30] J. Férec, M. Heniche, M.-C. Heuzey, G. Ausias, and P. Carreau, Numerical solution of the fokker–planck equation for fiber suspensions: application to the folgar–tucker–lipscomb model, Journal of non-newtonian fluid mechanics **155**, 20 (2008).

[31] M. Doi and S. Edwards, *The theory of polymer dynamics*, Vol. 73 (Oxford university press, 1988).

[32] H. K. Versteeg and W. Malalasekera, *An introduction to computational fluid dynamics: the finite volume method* (Pearson education, 2007).

[33] R. Alonso-Matilla, B. Ezhilan, and D. Saintillan, Microfluidic rheology of active particle suspensions: Kinetic theory, Biomicrofluidics **10** (2016).

[34] Y. Du, H. Jiang, and Z. Hou, Study of active brownian particle diffusion in polymer solutions, Soft Matter **15**, 2020 (2019).

[35] D. Ghernaout, A. I. Al-Ghonamy, A. Boucherit, B. Ghernaout, M. W. Naceur, N. A. Messaoudene, M. Aichouni, A. A. Mahjoubi, and N. A. Elboughdiri, Brownian motion and coagulation process, American Journal of Environmental Protection **4**, 1 (2015).

[36] D. Xu, R. Jia, Y. Li, and T. Gu, Advances in the treatment of problematic industrial biofilms, World Journal of Microbiology and Biotechnology **33**, 1 (2017).

[37] T. Rasamiravaka, Q. Labtani, P. Duez, M. El Jaziri, *et al.*, The formation of biofilms by pseudomonas aeruginosa: a review of the natural and synthetic compounds interfering with control mechanisms, BioMed research international **2015** (2015).

[38] P. Saxena, Y. Joshi, K. Rawat, and R. Bisht, Biofilms: architecture, resistance, quorum sensing and control mechanisms, Indian journal of microbiology **59**, 3 (2019).

[39] H. Issa, G. Natale, G. Ausias, and J. Férec, Modeling and numerical simulations of brownian rodlike particles with anisotropic translational diffusion, Physical Review Fluids **8**, 033302 (2023).

[40] G. L. Miño, M. D. Baabour, R. H. Chertcoff, G. O. Gutkind, E. Clément, H. Auradou, and I. P. Ippolito, E coli accumulation

behind an obstacle, (2018).